Condensation and Radial Transport of Filamentary Enstatite Crystals from Interplanetary Dust

Kainen Utt (k.l.utt@wustl.edu)
Washington University in St. Louis https://orcid.org/0000-0002-8555-9000
Ryan Ogliore
Washington University in St Louis
Nan Liu
Washington University in St. Louis https://orcid.org/0000-0002-4456-4065
Alexander Krot
University of Hawaii https://orcid.org/0000-0002-2278-8519
John Bradley
University of Hawaii at Manoa
Donald Brownlee
University of Washington
David Joswiak
University of Washington

Article

Keywords: interplanetary dust, enstatite whiskers, gas-solid condensation, nebular transport

Posted Date: January 28th, 2022

DOI: https://doi.org/10.21203/rs.3.rs-1243903/v1

Condensation and Radial Transport of Filamentary Enstatite Crystals from Interplanetary Dust

Kainen L. Utt[1,2*], Ryan C. Ogliore[1,2], Nan Liu[1,2], Alexander N. Krot[3], John P. Bradley[3], Donald E. Brownlee[4] and David J. Joswiak[4]

[1]Dept. of Physics, Washington Univ. in St. Louis, MO 63130.
[2]McDonnell Center for the Space Sciences, MO 63130.
[3]Hawaii Inst. of Geophysics & Planetology, Univ. of Hawaii at Mānoa, HI 96822.
[4]Dept. of Astronomy, Univ. of Washington, Seattle, WA 98195.

*Corresponding author(s). E-mail(s): k.l.utt@wustl.edu;

Abstract

Filamentary enstatite crystals, formed by gas-solid condensation in the solar nebula, are found in chondritic porous interplanetary dust particles of probable cometary origin. We measured the oxygen isotopic composition of four filamentary enstatite grains from the giant cluster interplanetary dust particle U2-20 GCP. These grains sample both the ^{16}O-rich solar ($\mathbf{\Delta}^{17}\mathrm{O} \approx \mathbf{-30}$ ‰) and ^{16}O-poor planetary ($\mathbf{\Delta}^{17}\mathrm{O} \approx \mathbf{0}$ ‰) isotope reservoirs. Our measurements provide evidence for very early vaporization of dust-poor and dust-rich regions of the solar nebula, followed by condensation and outward transport of crystalline dust to the comet-forming region very far from the Sun. Similar processes are likely responsible for the crystalline silicates observed in the outer regions of protoplanetary disks elsewhere in the Galaxy.

Keywords: interplanetary dust, enstatite whiskers, gas-solid condensation, nebular transport

Crystalline silicates are seen near and far from the central star in protoplanetary disks [1] and in comets, which formed in the outer Solar System [2, 3]. Interstellar dust is almost entirely amorphous [4], so it is thought that crystalline silicates in the outer regions of protoplanetary disks were either transported there from regions close to the central star (where stellar outbursts can vaporize disk material that then condenses as crystalline dust) or formed in situ via an energetic process in the outer disk [e.g., 5].

Outward transport from the inner Solar System to the comet-formation region is thought to have been inhibited by a gap at Jupiter's orbit as early as 1 Myr after CAIs based on high-precision bulk isotope measurements of meteorites [6] and astronomical observations of protoplanetary disks [7]. A chondrule-like fragment 'Iris' from comet Wild 2 was measured to have no detectable radiogenic ^{26}Mg from the decay of ^{26}Al ($t_{1/2}$ = 0.72 Myr). Iris was estimated to have formed very late in the solar nebula's lifetime —more than 3 Myr after calcium-aluminum-rich inclusions (CAIs) in CV chondrites with the canonical $^{26}Al/^{27}Al$ initial ratio of $5.2 \times 10^{-}5$. The mineralogy and O isotopic composition of Iris is similar to type II chondrules found in chondrites [8]. The existence of crystalline silicates in the outer regions of young protoplanetary disks, those that do not yet have gaps opened by forming planets, requires a mechanism distinct from those that formed chondrules like Iris.

Filamentary crystals were first predicted by Donn and Sears (1963) to form via vapor-to-solid condensation of nebular gas and be accreted into comets [9]. Roughly 20 years later, filamentary crystals (i.e., whiskers, ribbons, or platelets) of nearly iron-free clinoenstatite ($MgSiO_3$) were found in chondritic porous interplanetary dust particles (CP-IDPs) [10], which likely came from comets. In line with its predicted growth mechanism, cometary filamentary enstatite contains crystallographic defects indicative of direct condensation

from vapor (e.g., screw dislocations) and is elongated along the [100] crystallographic axis. As a consequence of having condensed directly from gas and escaped subsequent alteration (comets have experienced almost no thermal or aqueous processing), cometary filamentary enstatite reflects the isotopic composition of the gas from which it formed.

The oxygen isotopic composition of the Sun is ∼6 % enriched in ^{16}O compared to the terrestrial planets [11]. The likely astrophysical mechanism behind this solar-planetary difference is photochemical processing of the Solar System's parent molecular cloud by nearby massive stars [12]. Most CAIs and amoeboid olivine aggregates (AOAs), which likely condensed directly from gas very near the proto-Sun, have ^{16}O-rich isotopic compositions [13–15]. Chondrules, which likely formed in a dust-rich region of the disk [16], have roughly terrestrial or 'planetary' oxygen isotopic compositions [17]. Vaporizing a region of the nebula with an approximately solar dust-to-gas ratio (0.01) would produce a gas with roughly solar values of Δ^{17}O, whereas vaporizing a region with a greater-than-solar dust/gas ratio would produce a gas with higher Δ^{17}O values.

Prior to the Solar System's formation, the outer region of its parent molecular cloud was likely polluted by ^{26}Al-containing outflows from nearby Wolf-Rayet stars [18]. In the earliest stages of stellar evolution, before ^{26}Al had been homogenized throughout the disk, the mass accretion rate onto the proto-Sun was high and variable [19]. Fueled by this 'clumpy' mass accretion, the young proto-Sun likely emanated FU Orionis-like outbursts capable of vaporizing different regions of the disk [20] with variable dust/gas ratios [21, 22]. Un-melted fine-grained CAIs and AOAs lacking ^{26}Al are believed to have formed during this early stage and have variable oxygen isotopic compositions with $\Delta^{17}\mathrm{O} = -37$ ‰ to -5 ‰ [23]. CAIs that formed after ^{26}Al

homogenized (by which time FU Orionis-like outbursts were no longer common) are uniformly ^{16}O-rich ($\Delta^{17}O \approx -24$ ‰) [13–15], indicating that they likely formed near the Sun in a region with a roughly solar dust/gas ratio.

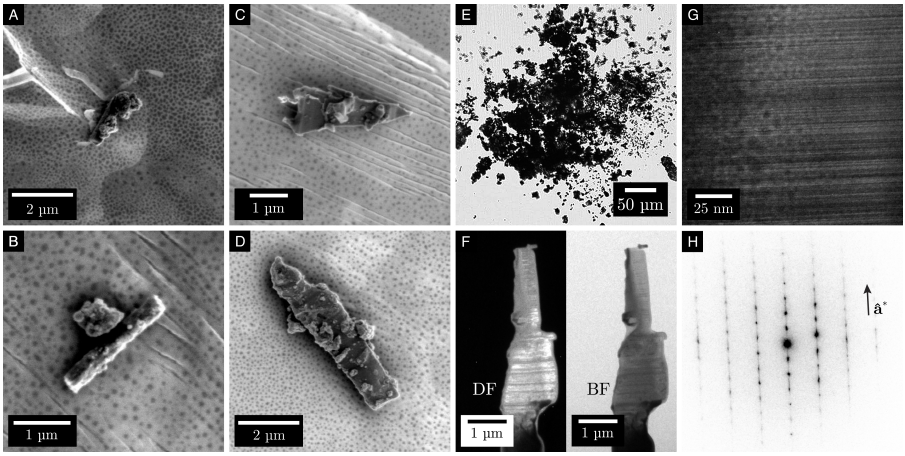

Fig. 1 (**A**–**D**) Secondary electron images of (A, B) enstatite whiskers and (C, D) enstatite ribbons. (**E**) Optical micrograph of U2-20 GCP, the giant cluster interplanetary dust particle that contains the filamentary enstatite crystals measured for oxygen isotopic compositions. (**F**) Bright- and dark-field TEM images (300 kV) of the enstatite ribbon shown in (D). These images show alternating high- and low-contrast bands indicative of stacking faults throughout the ribbon. (**G**) Higher magnification bright-field image of the same ribbon, displaying lattice fringes consistent with sporadic intergrowths of ortho- and clino-enstatite. (**H**) Inverted-contrast electron diffraction pattern from sample D. Severe streaking parallel to $\hat{\mathbf{a}}^*$ is consistent with stacking disorder and ortho/clino intergrowth.

Cluster IDPs are composed of unlithified, unequilibrated, and highly porous aggregates of compositionally diverse mineral fragments. CP-IDPs show some similarities to the Stardust samples returned from comet Wild 2 [e.g., 24] and to dust from comet 67P/Churyumov-Gerasimenko analyzed by the Rosetta mission [25]. For the giant cluster interplanetary dust particle chosen for this work (U2-20 GCP; Fig. 1E), multiple lines of evidence point towards a cometary origin (a brief summary of evidence supporting cometary origins for U2-20 can be found in the Supplementary Information). To investigate the origins of crystalline silicates in the comet-forming region, we measured the

oxygen isotopic compositions of four filamentary enstatite grains from U2-20 (Figs. 1A–D) using NanoSIMS scanning ion imaging of $^{16}O^-$, $^{17}O^-$, and $^{18}O^-$. Enstatite grains from the Norton County aubrite were used as isotope standards.

The acquired data are summarized in Table 1 and plotted on an oxygen three-isotope plot in Figure 2. Sample C is enriched in ^{16}O relative to Earth, with $\Delta^{17}O = -29.4 \pm 28.6$ ‰ and $\delta^{18}O = -73.3 \pm 12.8$ ‰ (2σ). Samples A, B, and D are consistent with a planetary oxygen isotopic composition and plot within 2σ of one another and a previously studied ribbon [26].

Table 1 Oxygen isotopic compositions, expressed in delta notation as per mill (‰) deviation from terrestrial, of four filamentary enstatite samples from U2-20 GCP. Listed 2σ uncertainties were calculated by bootstrap resampling methods.

Sample	Length (µm)	$\delta^{17}O \pm 2\sigma$	$\delta^{18}O \pm 2\sigma$	$\Delta^{17}O \pm 2\sigma$
A	1.8	-40.5 ± 46.3	0.5 ± 23.5	-40.7 ± 48.7
B	2.3	14.6 ± 83.6	-11.5 ± 69.1	20.6 ± 89.5
C	3.4	-67.6 ± 27.9	-73.3 ± 12.8	-29.4 ± 28.6
D	6.1	-6.8 ± 20.1	-2.8 ± 8.9	-5.4 ± 20.4

High-magnification bright-field TEM images of sample D (Fig. 1G) exhibit alternating high- and low-contrast bands that indicate stacking faults caused by the sporadic intergrowth of ortho- and clino-enstatite. These stacking faults are also indicated by the intense streaking parallel to the $\hat{\mathbf{a}}^*$-axis visible in the electron diffraction pattern. These crystallographic features suggest this ribbon condensed from a high-temperature vapor, forming proto-enstatite that converted to ortho-/clino-enstatite as it cooled [10].

Sample C is among the most ^{16}O-enriched Solar System objects ever measured: it plots within 2σ of the O isotopic composition of the Sun as inferred from Genesis measurements [11] and exceedingly rare ^{16}O-rich refractory inclusions in carbonaceous chondrites [13, 15]. Sample C's extremely ^{16}O-rich

composition is consistent with condensation from a gas produced by evaporation of a disk region with a roughly solar dust/gas ratio, likely near the central star or above the disk's mid-plane [20]. Samples A, B, and D and a previously studied ribbon from the same cluster [26] have 'planetary' oxygen isotopic compositions that plot within 2σ of $\delta^{17,18}O = 0$. Samples A and D are inconsistent, at the $>2\sigma$ level, with sample C and ^{16}O-rich gas-to-solid condensates/refractory inclusions found in meteorites. The O isotopic compositions of samples A, C, and D suggest that they formed by re-condensation of vaporized dust-rich regions of the disk, possibly near the terrestrial planet-forming region where ^{16}O-poor solids were abundant.

Both ^{16}O-poor and ^{16}O-rich filamentary enstatite could condense in the inner disk if both groups formed early. Oxygen isotope measurements of a hibonite-rich, fine-grained CV3 CAI are consistent with coexisting primordial ^{16}O-poor and ^{16}O-rich gaseous reservoirs [29]. We propose that the ^{16}O-poor and ^{16}O-rich filamentary enstatite reported here were formed similarly—by vaporization of different regions of the solar nebula by FU Orionis-like outbursts, when mass accretion rates on the Sun were highest (i.e., very early). Filamentary enstatite crystals that condensed from these different gas reservoirs were transported to the outer regions of the disk and subsequently accreted by the same (likely cometary) parent body.

The rate of outward transport in a protoplanetary disk is roughly proportional to the rate of mass accretion onto the central star [19, 20]. Grains that condensed early and close to the Sun would be efficiently transported outwards. Outer Solar System bodies such as comets likely accreted some of the oldest crystalline dust that formed close to the Sun. The migration of inner Solar System likely took place in the first ~500 kyr, before Jupiter's core opened a

gap in the disk [30]. A schematic of the formation and transport of filamentary enstatite to the comet forming region is shown in Figure 3.

Our results can explain the isotopic composition of refractory inclusions in outer Solar System bodies and the origin of crystalline dust in young disks elsewhere in the Galaxy. For example, the refractory particle 'Inti' from comet Wild 2 lacks radiogenic ^{26}Mg [31] and is ^{16}O-rich with $\Delta^{17}O \approx -20$ ‰ [27]. We interpret Inti's lack of radiogenic ^{26}Mg as a sign of early formation and predict that similar refractory objects in comets should be free of radiogenic ^{26}Mg and have variable Δ^{17}O values. A similar scenario can explain CAIs in CH chondrites, whose parent-body accreted late and far from the Sun. Compared to other meteorite classes, CH chondrites contain a high proportion of ^{26}Al-poor CAIs, which formed close to the young Sun and exhibit a range of Δ^{17}O values [23, 32]. Using the Solar System as a general model for planet formation in the Galaxy, crystalline dust observed in the outer regions of extrasolar protoplanetary disks [1] could have formed and migrated outward early in the disk's lifetime.

Acknowledgments This work was funded by NASA grant NNX14AF22G. The data and Matlab program used for this work are publicly available (DOI: 10.6084/m9.figshare.16766557.v4). The authors declare that they have no competing interests.

Author Contributions:

Conceptualization: KLU, RCO, JPB, DEB, DJJ

Data Curation: KLU, RCO

Formal Analysis: KLU, RCO

Methodology: KLU, RCO, NL, JPB

Investigation: KLU, RCO, NL, JPB

Visualization: KLU

Resources: JPB, DEB, DJJ

Project Administration: RCO

Funding Acquisition: RCO

Supervision: RCO, ANK, JPB, DEB, DJJ

Writing—Original Draft: KLU, RCO

Writing—Review & Editing: KLU, RCO, NL, ANK, JPB, DEB, DJJ

Materials and Methods Each sample was transferred to a sputter-cleaned Au foil mount using a computer-controlled Omniprobe micro-manipulator equipped on an FEI Quanta 3D FIB. Within a 10 µm radius of each sample, we placed three grains from a crushed sample of the Norton County aubrite. This geometry allowed for simultaneous measurements of the sample and internal standards.

We acquired 12×12-µm, 256×256-pixel ion raster images using the Wash U Cameca NanoSIMS 50. Each sample was pre-sputtered with a 78 pA Cs^+ beam for 300 s to remove any adsorbed water or insoluble organic matter. Measurements were collected using a 2 pA Cs^+ primary beam focused to approximately 100 nm. We simultaneously collected $^{16}O^-$, $^{17}O^-$, and $^{18}O^-$ on separate electron multipliers. In addition to O isotopes, we collected $^{12}C^-$ and $^{13}C^-$, which incidentally allowed us to monitor the pre-sputtering progress. No carbon isotopic anomalies were observed. For all four samples, the mass-resolving power for $^{17}O^-$ was $\gtrsim$5500, sufficient to resolve the interference from $^{16}OH^-$. We collected 90–100 frames (2.5 hr) for each sample, after which the whiskers (samples A and B) were entirely consumed. However, material from the ribbons (samples C and D) remained after the measurements.

Isotopic data were analyzed using a custom Matlab script. Un-processed data and the script used to analyse them (including ROIs used and all other dependent files) are available for public download [33]. We aligned the images

from each cycle and defined regions of interest (ROIs), avoiding grain- and raster-edges to reduce topography-induced instrumental fractionation effects. The ROIs were also drawn to avoid any adhering grains or potential contamination that remained after pre-sputtering. The aligned data was then summed for each ROI to calculate the isotopic ratios $^{17}O/^{16}O$ and $^{18}O/^{16}O$. These raw ratios were used to calculate delta-values referenced to simultaneously measured NC aubrite standard grains via:

$$\delta^{17,18}\mathrm{O} = \left[\frac{\left(\frac{^{17,18}\mathrm{O}}{^{16}\mathrm{O}}\right)_u \left(\frac{^{17,18}\mathrm{O}}{^{16}\mathrm{O}}\right)^{\mathrm{s}}_{\mathrm{k}}}{\left(\frac{^{17,18}\mathrm{O}}{^{16}\mathrm{O}}\right)^{\mathrm{s}}_{\mathrm{m}} \left(\frac{^{17,18}\mathrm{O}}{^{16}\mathrm{O}}\right)_{\mathrm{VS}}} - 1 \right] \times 1000 \tag{1}$$

where $(^{17,18}O/^{16}O)_u$ is the measured ratio of the unknown, $(^{17,18}O/^{16}O)^s{}_m$ is the ratio of the simultaneously-measured standards, $(^{17,18}O/^{16}O)^s{}_k$ is the accepted literature value for NC enstatite, and $(^{17,18}O/^{16}O)^s{}_{VS}$ is the accepted value for Vienna Standard Mean Ocean Water [34]. Norton County has an oxygen isotopic composition (relative to VSMOW) of $\delta^{17}O = 2.77 \pm 0.04$ ‰, $\delta^{18}O = 5.28 \pm 0.08$ ‰, and $\Delta^{17}O = 0.0044 \pm 0.005$ ‰ [35–37]. VSMOW has isotopic ratios of $^{17}O/^{16}O = 0.0003829$ and $^{18}O/^{16}O = 0.00200052$ [38, 39]. Calculating delta-values in this way minimizes multiplicative confounding factors, such as instrumental mass fractionation (IMF), quasi-simultaneous arrival (QSA), and detector dead time. The reported uncertainties were calculated via bootstrap resampling (10^6 trials with replacement) of the pixels within each ROI. The calculated bootstrap uncertainties were found to be greater than or equal to statistical, though the deviation was found to be minimal in most cases. This method for calculating the uncertainty is more likely to yield a reliable estimate for a small number of counts and is therefore more appropriate for the small size of the studied samples (and resulting small number of total counts).

After NanoSIMS measurements, we prepared the remaining portions of samples C and D for analysis via transmission electron microscopy (TEM). Using the Omniprobe micro-manipulator, we transferred the ribbon remnants from the Au-foil substrate to a liftout grid to which they were secured with a thin Pt weld. The samples were subsequently thinned to electron transparency (∼200 nm thick) and briefly polished with a 5 kV, 48 pA Ga^+ beam (∼30 s per side). Throughout the process, the Ga^+ ion beam was used only sparingly to minimize potential amorphization effects.

Electron diffraction measurements were performed with the FEI Titan3 G2 60-300 dual aberration-corrected TEM/STEM at the Advanced Electron Microscopy Center, University of Hawaii at Mānoa. Bright- and dark-field images and electron diffraction patterns were collected for the remnants of samples C and D, however, only sample D contained enough undamaged material to extract crystallographic information. The remnants of sample C had been too thoroughly amorphized during the NanoSIMS measurements.

References

[1] D. Apai, I. Pascucci, J. Bouwman, A. Natta, T. Henning, C.P. Dullemond, The onset of planet formation in brown dwarf disks. Science **310**(5749), 834–836 (2005). https://doi.org/10.1126/science.1118042

[2] M.E. Zolensky, T.J. Zega, H. Yano, S. Wirick, A.J. Westphal, M.K. Weisberg, I. Weber, J.L. Warren, M.A. Velbel, A. Tsuchiyama, P. Tsou, A. Toppani, N. Tomioka, K. Tomeoka, N. Teslich, M. Taheri, J. Susini, R. Stroud, T. Stephan, F.J. Stadermann, C.J. Snead, S.B. Simon, A. Simionovici, T.H. See, F. Robert, F.J.M. Rietmeijer, W. Rao, M.C. Perronnet, D.A. Papanastassiou, K. Okudaira, K. Ohsumi, I. Ohnishi, K. Nakamura-Messenger, T. Nakamura, S. Mostefaoui, T. Mikouchi,

A. Meibom, G. Matrajt, M.A. Marcus, H. Leroux, L. Lemelle, L. Le, A. Lanzirotti, F. Langenhorst, A.N. Krot, L.P. Keller, A.T. Kearsley, D. Joswiak, D. Jacob, H. Ishii, R. Harvey, K. Hagiya, L. Grossman, J.N. Grossman, G.A. Graham, M. Gounelle, P. Gillet, M.J. Genge, G. Flynn, T. Ferroir, S. Fallon, D.S. Ebel, Z.R. Dai, P. Cordier, B. Clark, M. Chi, A.L. Butterworth, D.E. Brownlee, J.C. Bridges, S. Brennan, A. Brearley, J.P. Bradley, P. Bleuet, P.A. Bland, R. Bastien, Mineralogy and petrology of Comet 81P/Wild 2 nucleus samples. Science **314**(5806), 1735–1739 (2006). https://doi.org/10.1126/science.1135842

[3] D. Brownlee, D. Joswiak, G. Matrajt, Overview of the rocky component of Wild 2 comet samples: Insight into the early solar system, relationship with meteoritic materials and the differences between comets and asteroids. Meteoritics & Planetary Science **47**(4), 453–470 (2012). https://doi.org/10.1111/j.1945-5100.2012.01339.x

[4] F. Kemper, W.J. Vriend, A.G.G.M. Tielens, The Absence of Crystalline Silicates in the Diffuse Interstellar Medium. The Astrophysical Journal **609**(2), 826–837 (2004). https://doi.org/10.1086/421339

[5] J.C. Bridges, H.G. Changela, S. Nayakshin, N.A. Starkey, I.A. Franchi, Chondrule fragments from Comet Wild 2: Evidence for high temperature processing in the outer Solar System. Earth and Planetary Science Letters **341-344**, 186–194 (2012). https://doi.org/10.1016/j.epsl.2012.06.011

[6] T.S. Kruijer, C. Burkhardt, G. Budde, T. Kleine, Age of Jupiter inferred from the distinct genetics and formation times of meteorites. Proceedings of the National Academy of Sciences **114**(26), 6712–6716 (2017). https://doi.org/10.1073/pnas.1704461114

[7] M. Ansdell, J.P. Williams, N. van der Marel, J.M. Carpenter, G. Guidi, M. Hogerheijde, G.S. Mathews, C.F. Manara, A. Miotello, A. Natta, I. Oliveira, M. Tazzari, L. Testi, E.F. van Dishoeck, S.E. van Terwisga, ALMA survey of Lupus protoplanetary disks. I. Dust and gas masses. The Astrophysical Journal **828**(1), 46 (2016). https://doi.org/10.3847/0004-637x/828/1/46

[8] R.C. Ogliore, G.R. Huss, K. Nagashima, A.L. Butterworth, Z. Gainsforth, J. Stodolna, A.J. Westphal, D. Joswiak, T. Tyliszczak, Incorporation of a Late-Forming Chondrule into Comet Wild 2. The Astrophysical Journal **745**(2), L19 (2012). https://doi.org/10.1088/2041-8205/745/2/l19

[9] B. Donn, G.W. Sears, Planets and comets: role of crystal growth in their formation. Science **140**(3572), 1208–1211 (1963). https://doi.org/10.1126/science.140.3572.1208

[10] J. Bradley, D. Brownlee, D. Veblen, Pyroxene whiskers and platelets in interplanetary dust: evidence of vapour phase growth. Nature **301**(5900), 473–477 (1983). https://doi.org/10.1038/301473a0

[11] K.D. McKeegan, A.P.A. Kallio, V.S. Heber, G. Jarzebinski, P.H. Mao, C.D. Coath, T. Kunihiro, R.C. Wiens, J.E. Nordholt, R.W. Moses, D.B. Reisenfeld, A.J.G. Jurewicz, D.S. Burnett, The oxygen isotopic composition of the Sun inferred from captured solar wind. Science **332**(6037), 1528–1532 (2011). https://doi.org/10.1126/science.1204636

[12] L.G. Vacher, R.C. Ogliore, C. Jones, N. Liu, D.A. Fike, Cosmic symplectite recorded irradiation by nearby massive stars in the solar system's parent molecular cloud. Geochimica et Cosmochimica Acta **309**, 135–150 (2021). https://doi.org/10.1016/j.gca.2021.06.026

[13] A.N. Krot, K.D. McKeegan, L.A. Leshin, G.J. MacPherson, E.R.D. Scott, Existence of an ^{16}O-rich gaseous reservoir in the solar nebula. Science **295**(5557), 1051–1054 (2002). https://doi.org/10.1126/science.1068200

[14] M. Gounelle, A.N. Krot, K. Nagashima, A. Kearsley, Extreme ^{16}O enrichment in calcium-aluminum-rich inclusions from the Isheyevo (CH/CB) chondrite. The Astrophysical Journal **698**(1), L18–L22 (2009). https://doi.org/10.1088/0004-637x/698/1/l18

[15] L. Kööp, K. Nagashima, A.M. Davis, A.N. Krot, A refractory inclusion with solar oxygen isotopes and the rarity of such objects in the meteorite record. Meteoritics & Planetary Science **55**(3), 524–534 (2020). https://doi.org/10.1111/maps.13434

[16] S.J. Desch, H.C. Connolly, A model of the thermal processing of particles in solar nebula shocks: Application to the cooling rates of chondrules. Meteoritics & Planetary Science **37**(2), 183–207 (2002). https://doi.org/10.1111/j.1945-5100.2002.tb01104.x

[17] N.T. Kita, H. Nagahara, S. Tachibana, S. Tomomura, M.J. Spicuzza, J.H. Fournelle, J.W. Valley, High precision SIMS oxygen three isotope study of chondrules in LL3 chondrites: Role of ambient gas during chondrule formation. Geochimica et Cosmochimica Acta **74**(22), 6610–6635 (2010). https://doi.org/10.1016/j.gca.2010.08.011

[18] F.C. Pignatale, E. Jacquet, M. Chaussidon, S. Charnoz, Fingerprints of the protosolar cloud collapse in the Solar System. I. Distribution of presolar short-lived ^{26}Al. The Astrophysical Journal **884**(1), 31 (2019). https://doi.org/10.3847/1538-4357/ab3c1f

[19] P.J. Armitage, M. Livio, J.E. Pringle, Episodic accretion in magnetically layered protoplanetary discs. Monthly Notices of the Royal Astronomical Society **324**(3), 705–711 (2001). https://doi.org/10.1046/j.1365-8711.2001.04356.x

[20] A.P. Boss, C.M.O. Alexander, M. Podolak, Evolution of CAI-sized particles during FU Orionis outbursts. I. Particle trajectories in protoplanetary disks with beta cooling. The Astrophysical Journal **901**(1), 81 (2020). https://doi.org/10.3847/1538-4357/abafb9

[21] F.C. Pignatale, S. Charnoz, M. Chaussidon, E. Jacquet, Making the Planetary Material Diversity during the Early Assembling of the Solar System. The Astrophysical Journal **867**(2), L23 (2018). https://doi.org/10.3847/2041-8213/aaeb22

[22] K.L. Soon, M. Momose, T. Muto, T. Tsukagoshi, A. Kataoka, T. Hanawa, M. Fukagawa, K. Saigo, H. Shibai, Investigating the gas-to-dust ratio in the protoplanetary disk of HD 142527. Publications of the Astronomical Society of Japan (2019). https://doi.org/10.1093/pasj/psz112

[23] A.N. Krot, K. Nagashima, E.M.M. van Kooten, M. Bizzarro, Calcium-aluminum-rich inclusions recycled during formation of porphyritic chondrules from CH carbonaceous chondrites. Geochimica et Cosmochimica Acta **201**, 185–223 (2017). https://doi.org/10.1016/j.gca.2016.09.001

[24] R.C. Ogliore, R.L. Palma, J. Stodolna, K. Nagashima, R.O. Pepin, D.J. Schlutter, Z. Gainsforth, A.J. Westphal, G.R. Huss, Q-gases in a late-forming refractory interplanetary dust particle: A link to comet Wild 2. Geochimica et Cosmochimica Acta **271**, 116–131 (2020). https://doi.org/10.1016/j.gca.2019.11.033

[25] T. Mannel, M.S. Bentley, P.D. Boakes, H. Jeszenszky, P. Ehrenfreund, C. Engrand, C. Koeberl, A.C. Levasseur-Regourd, J. Romstedt, R. Schmied, K. Torkar, I. Weber, Dust of comet 67P/Churyumov-Gerasimenko collected by Rosetta/MIDAS: classification and extension to the nanometer scale. Astronomy & Astrophysics **630**, A26 (2019). https://doi.org/10.1051/0004-6361/201834851

[26] R.C. Ogliore, D.E. Brownlee, K. Nagashima, D.J. Joswiak, J.B. Lewis, A.N. Krot, K.L. Utt, G.R. Huss, Oxygen isotopic composition of an enstatite ribbon of probable cometary origin. Meteoritics & Planetary Science **55**(6), 1371–1381 (2019). https://doi.org/10.1111/maps.13364

[27] K.D. McKeegan, J. Aléon, J. Bradley, D. Brownlee, H. Busemann, A. Butterworth, M. Chaussidon, S. Fallon, C. Floss, J. Gilmour, M. Gounelle, G. Graham, Y. Guan, P.R. Heck, P. Hoppe, I.D. Hutcheon, J. Huth, H. Ishii, M. Ito, S.B. Jacobsen, A. Kearsley, L.A. Leshin, M.C. Liu, I. Lyon, K. Marhas, B. Marty, G. Matrajt, A. Meibom, S. Messenger, S. Mostefaoui, S. Mukhopadhyay, K. Nakamura-Messenger, L. Nittler, R. Palma, R.O. Pepin, D.A. Papanastassiou, F. Robert, D. Schlutter, C.J. Snead, F.J. Stadermann, R. Stroud, P. Tsou, A. Westphal, E.D. Young, K. Ziegler, L. Zimmermann, E. Zinner, Isotopic compositions of cometary matter returned by stardust. Science **314**(5806), 1724–1728 (2006). https://doi.org/10.1126/science.1135992

[28] R.C. Ogliore, K. Nagashima, G.R. Huss, A.J. Westphal, Z. Gainsforth, A.L. Butterworth, Oxygen isotopic composition of coarse- and fine-grained material from comet 81P/Wild 2. Geochimica et Cosmochimica Acta **166**, 74–91 (2015). https://doi.org/10.1016/j.gca.2015.04.028

[29] S. Wada, N. Kawasaki, C. Park, H. Yurimoto, Melilite condensed from an ^{16}O-poor gaseous reservoir: Evidence from a fine-grained Ca-Al-rich inclusion of Northwest Africa 8613. Geochimica et Cosmochimica Acta **288**, 161–175 (2020). https://doi.org/10.1016/j.gca.2020.08.004

[30] F.J. Ciesla, The distributions and ages of refractory objects in the solar nebula. Icarus **208**(1), 455–467 (2010). https://doi.org/10.1016/j.icarus.2010.02.010

[31] J.E.P. Matzel, H.A. Ishii, D. Joswiak, I.D. Hutcheon, J.P. Bradley, D. Brownlee, P.K. Weber, N. Teslich, G. Matrajt, K.D. McKeegan, G.J. MacPherson, Constraints on the formation age of cometary material from the NASA Stardust mission. Science **328**(5977), 483–486 (2010). https://doi.org/10.1126/science.1184741

[32] E.M.M.E. van Kooten, D. Wielandt, M. Schiller, K. Nagashima, A. Thomen, K.K. Larsen, M.B. Olsen, Å. Nordlund, A.N. Krot, M. Bizzarro, Isotopic evidence for primordial molecular cloud material in metal-rich carbonaceous chondrites. Proceedings of the National Academy of Sciences **113**(8), 2011–2016 (2016). https://doi.org/10.1073/pnas.1518183113

[33] K. Utt, Oxygen isotope measurements of cometary filamentary enstatite. Dataset, Figshare (2021). https://doi.org/10.6084/m9.figshare.16766557.v4

[34] R. Ogliore, K. Nagashima, G. Huss, P. Haenecour, A reassessment of the quasi-simultaneous arrival effect in secondary ion mass spectrometry. Nuclear Instruments and Methods in Physics Research Section B: Beam Interactions with Materials and Atoms **491**, 17–28 (2021). https://doi.

org/10.1016/j.nimb.2021.01.007

[35] R.N. Clayton, T.K. Mayeda, A.E. Rubin, Oxygen isotopic compositions of enstatite chondrites and aubrites. Journal of Geophysical Research **89**(S01), C245 (1984). https://doi.org/10.1029/jb089is01p0c245

[36] Y.N. Miura, H. Hidaka, K. Nishiizumi, M. Kusakabe, Noble gas and oxygen isotope studies of aubrites: A clue to origin and histories. Geochimica et Cosmochimica Acta **71**(1), 251–270 (2007). https://doi.org/10.1016/j.gca.2006.07.040

[37] J. Newton, I.A. Franchi, C.T. Pillinger, The oxygen-isotopic record in enstatite meteorites. Meteoritics & Planetary Science **35**(4), 689–698 (2000). https://doi.org/10.1111/j.1945-5100.2000.tb01452.x

[38] K. Lodders, B. Fegley, Jr., *The Planetary Scientist's Companion* (Oxford University Press, 1998)

[39] M. Kusakabe, Y. Matsuhisa, Oxygen three-isotope ratios of silicate reference materials determined by direct comparison with VSMOW-oxygen. Geochemical Journal **42**(4), 309–317 (2008). https://doi.org/10.2343/geochemj.42.309

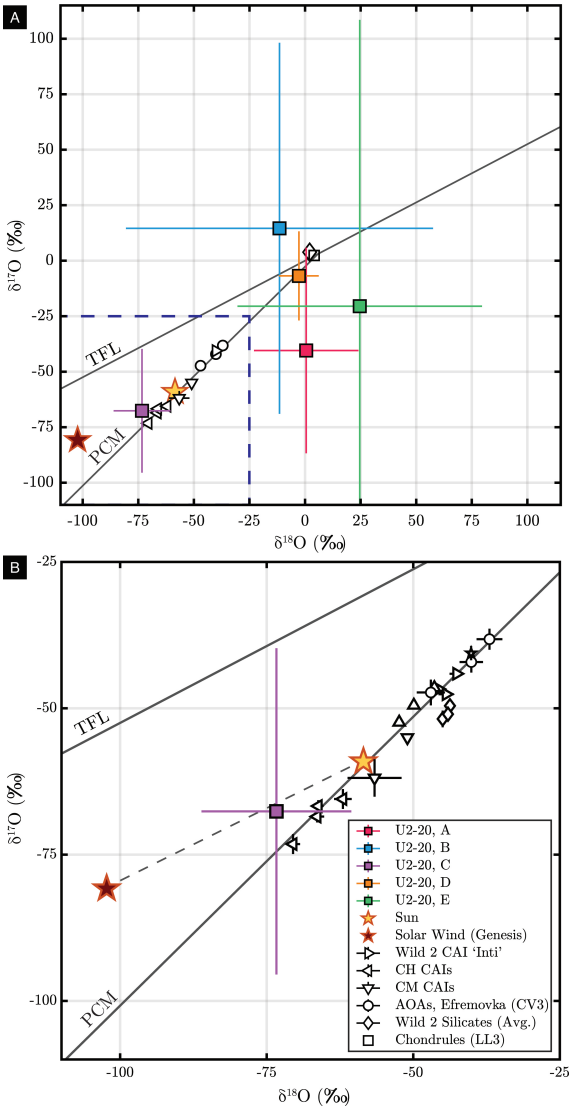

Fig. 2 (**A**) Oxygen three-isotope plot of U2-20 filamentary enstatite samples (U2-20, A–D). Uncertainties are 2σ. Also plotted: a ribbon (U2-20, E) from the same cluster [26], *Genesis* solar measurements [11], amoeboid olivine aggregates (AOAs) from Efremovka [13], chondrules (LL3) [17], a CAI-like object ('Inti') found in comet Wild 2 [27], mean comet Wild 2 fines [28], CH CAIs [14, 23], and CM CAIs [15]. (**B**) Zoom-in of the dashed region in (A). TFL, terrestrial fractionation line; PCM, primitive chondrule mineral line.

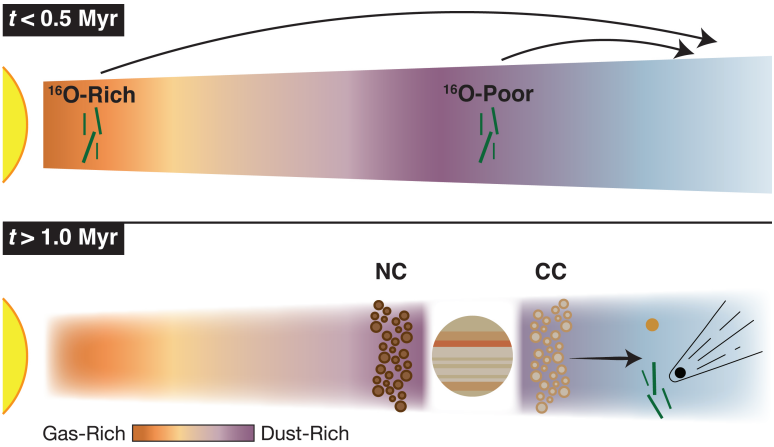

Fig. 3 Illustration of the proposed formation and transport of filamentary enstatite grains with dichotomous oxygen isotopic compositions. The grains were transported from different regions of the inner disk to the outer disk quickly after they formed, and before a forming Jupiter opened a gap in the disk. The cometary and asteroidal parent bodies (NC, non-carbonaceous; CC, carbonaceous chondrites) formed from material that was local to different regions of the solar nebula at the time they formed [6].

Supplementary Files

This is a list of supplementary files associated with this preprint. Click to download.

- NatureFilamentaryEnSI.pdf